JOURNAL OF MATERIALS SCIENCE 28 (1993) 1901–1909

# The effect of surface-limited microcracks on the effective Young's modulus of ceramics

## Part II *Application of analysis to particular microcrack geometries*

Y. KIM, E. D. CASE
*Department of Metallurgy, Mechanics and Materials Science, Michigan State University, East Lansing, MI 48824-1226, USA*

This paper considers the details of crack orientation and crack geometry effects on the dynamic modulus model and the rule-of-mixtures model developed in Part I for surface-limited microcracking damage in ceramics. In particular, the implications of using indentation cracks as a model crack system are considered, including accommodation of the hemispherically deformed zone ligament that bridges part of the opposing crack surfaces for indentation crack systems.

## 1. Introduction

In Part I [1], the authors modelled surface-limited microcrack damage in terms of the elastic modulus of a composite bar. The microcracked bar was viewed as a two- or three-layer composite, with the microcracked layer(s) having a reduced elastic modulus (Fig. 1 in Part I [1]). The fractional modulus change for a surface-microcracked bar was modelled in terms of: (i) a rule of mixtures (ROM) formulation, which implies a static, tensile measurement of modulus and by (ii) the Bernoulli–Euler beam equation, which is appropriate to a dynamic elastic modulus measurement of the overall modulus [1]. The ROM and dynamic modulus expressions were thus functions of $E_\ell$, the elastic modulus of the microcracked layer. To express the composite (overall) modulus explicitly in terms of microcrack parameters, $E_\ell$ was expressed directly in terms of microcrack orientation, geometry and number density.

In this study we consider the effect of particular crack geometries and crack orientations, including a "model" crack field produced by a distribution of indentation cracks.

## 2. Generalized models for surface-limited microcrack damage

For convenience, the authors' previous expressions for surface-limited microcracking [1] are highlighted in Equations 1 and 2 below. The three-layer ROM model [1] consists of two microcracked surface layers having moduli $E_{\ell 1}$ and $E_{\ell 2}$ and an intermediate, undamaged layer of modulus $E_s$. The relative change in modulus may be expressed as

$$\frac{E_s - \bar{E}_{3_{ROM}}}{E_s} = v_{\ell 1} f_1 G_{\ell 1} N_{\ell 1} + v_{\ell 2} f_2 G_{\ell 2} N_{\ell 2} \quad (1)$$

where $v_{\ell 1}$, $v_{\ell 2}$ = volume fraction of microcracked layer 1 and microcracked layer 2, respectively, $f_1$, $f_2$ = crack orientation function for the cracks in microcracked layer 1 and microcracked layer 2, respectively, $G_{\ell 1}$, $G_{\ell 2}$ = crack geometry factor $2\langle A^2\rangle/\pi\langle P\rangle$ for the cracks in microcracked layer 1 and microcracked layer 2, respectively, and $N_{\ell 1}$, $N_{\ell 2}$ = number density of microcracks in microcracked layer 1 and microcracked layer 2, respectively. The two-layer ROM case (one microcracked layer and one undamaged layer) for the relative modulus change is given by the first term in the sum on the right-hand side of Equation 1.

The three-layer dynamic modulus model [1] again consists of two microcracked surface layers having moduli $E_{\ell 1}$ and $E_{\ell 2}$ and an intermediate, undamaged layer of modulus $E_s$ where the relative modulus change may be expressed as

$$\frac{E_s - \bar{E}_{3_{DYN}}}{E_s} = \frac{R_1[R_1^2 + 3(R_2 + 1)^2] f_1 G_{\ell 1} N_{\ell 1} + R_2[R_2^2 + 3(R_1 + 1)^2] f_2 G_{\ell 2} N_{\ell 2}}{(R_1 + R_2 + 1)^3} \quad (2)$$

where $R_1 = d_{\ell 1}/d_s$, $R_2 = d_{\ell 2}/d_s$. If $d_{\ell 2} = 0$, then $R_2 = 0$ and Equation 2 applies for the two-layer model consisting of one microcracked layer and an undamaged layer [1].

## 3. Selection of microcracking models for use with the generalized expression of surface-limited microcracking

As expressed above, the ROM and dynamic modulus models can be expressed in terms of any one of a number of microcracking theories [2–6]. It should be emphasized that to obtain Equations 1 and 2 we first

0022–2461  

modelled a body having surface-limited microcracking as a layered composite with an undamaged layer and a layer (or layers) having reduced modulus, where the reduced modulus represents the effects of microcracking in the surface layers [1]. Microcracking within the surface layer then can be expressed in terms of available theories for microcracks whose centroids are (on average) homogeneously distributed in space [2–5].

Budiansky and O'Connell [2], Salganik [3], Hoenig [4], and Laws and Brockenbrough [5] each express the effective Young's modulus $E$ of the microcracked body as

$$E = E_s(1 - f\varepsilon) \quad (3)$$

where $E_s$ refers to the non-microcracked Young's modulus. The function $f$ depends on the spatial orientation of the microcracks (Table I). The crack damage parameter $\varepsilon$ can be expressed [2–5] as

$$\varepsilon = \frac{2}{\pi}\left(\frac{\langle A^2\rangle}{\langle P\rangle}\right)N_v = GN_v \quad (4)$$

where $N_v$ = volume number density of microcracks, $\langle A^2\rangle$ = mean of the square of the crack surface area, $\langle P\rangle$ = mean crack perimeter and $G$ = crack geometry parameter. Thus the crack damage parameter $\varepsilon$ can be expressed as a function of the microcrack volume number density $N_v$, the crack geometry, and the crack dimensions. In this paper we shall use the product $GN_v$ as our crack damage parameter rather than $\varepsilon$, since we seek to emphasize the functional relationships between microcrack geometry and crack number density.

The microcracking-modulus theories of Budiansky and O'Connell [2], Salganik [3], Hoenig [4], and Laws and Brockenbrough [5] are linearly dependent on the crack damage parameter $\varepsilon$ (Equation 4), and hence these theories [2–5] may be termed "linear modulus decrement models". The variational technique developed by Willis [6], which in turn is based on the Hashin–Strikman method, is a higher-order microcracking-modulus decrement theory. While Willis's theory may allow calculations of modulus decrements for somewhat higher crack number densities within a damaged surface layer, Willis's expressions are mathematically unwieldily and thus in this study we employed the linear microcracking theories.

Differences between the four linear microcracking theories include the treatment of the spatial alignment of microcracks. Budiansky and O'Connell [2] and Salganik [3] deal with randomly oriented microcrack populations only, Hoenig [4] treats aligned microcracks, and Laws and Brockenbrough [5] treat both randomly oriented and aligned microcrack populations. While in each of the four theories the alignment function $f$ is expressed as a function of Poisson's ratio, Budiansky and O'Connell [2] express $f$ as a function of both $\nu$ (Poisson's ratio of the microcracked state) and $\nu_0$ (Poisson's ratio of the non-microcracked state). Salganik [3] and Laws and Brockenbrough [5] express $f$ in terms of $\nu_0$ only. Despite these apparent differences in the form of $f$, the values of $f$ differ little from one another for realistic ranges of $\nu$ and $\nu_0$ [7]. Thus, the linear microcracking theories [2–5] are quite similar. In order to treat particular microcrack geometries, we chose to describe the layer modulus in terms of Laws and Brockenbrough's model [5]. Table I summarizes Laws and Brockenbrough's [5] microcracking relations, which include "standard" crack geometries of circular, elliptical, and slot-type crack geometries.

## 4. Relative crack size versus layer depth considerations

The nature of the microcracked surface layer(s) for particular microcracked bodies can be classified in terms of the mean microcrack size $\langle c\rangle$ and the depth of the microcrack damage layer, $d_\ell$. In this paper, we shall consider two limits of relative crack/layer depth.

If $\langle c\rangle \ll d_\ell$, then the microcracked layer itself can be considered to be a three-dimensional body. Within the microcracked layer, the implicit assumption [2–7] that the microcracks are distributed homogeneously in space (over size scales large compared to $\langle c\rangle$, the mean crack dimension) may or may not be valid*. If microcracks are distributed homogeneously on average, and if the crack alignment, crack geometry and crack number density in the layer(s) can be determined or estimated, then the effective modulus of the microcracked layer can be calculated based on the linear modulus–microcracking relationships [2–6]. The effective elastic modulus of the entire specimen can then be calculated based on the rule-of-mixtures model or the dynamic modulus model developed by the authors (Equations 1 and 2 in section 2). The case that $\langle c\rangle \ll d_\ell$ could correspond physically, for example, to a microcracked specimen in which the microcrack-damaged surface layer(s) resulted from a martensitic-type phase transformation. Alternatively, the case that $\langle c\rangle \ll d_\ell$ might correspond to a layered composite specimen in which the layers were microcracked‡.

A second asymptote for the crack size versus layer depth relation is the case that $\langle c\rangle = d_\ell$, where the crack layer depth is defined by the penetration of the cracks in the microcracked layer (assuming the cracks are oriented perpendicular to the specimen surface). This case might correspond to, for example, a surface crack array formed via surface grinding [9–11] or thermal shock of a brittle material. Alternatively, $\langle c\rangle = d_\ell$ might correspond to a crack field formed by

*Homogeneous distribution in space refers here to the location of the centroids of the crack surfaces. Homogeneous spatial distribution makes no assumptions about the mutual orientation of the crack faces. Thus microcracks can be, on average, homogeneously distributed in space but oriented parallel to one another, oriented randomly with respect to one another, or oriented in some intermediate, partially aligned state.

‡If the layer's grain size were much smaller than the layer thickness, microcracks induced by thermal expansion anisotropy or phase transformations would probably be much smaller on average than the layer thickness [8].

an array of indentation cracks on one or more specimen surfaces.

Although indentation cracks have been used as model cracks in a number of studies, the detailed morphology of indentation cracks is not included in the crack geometries (circular, elliptical and slot, as listed in Table I) typically considered in microcrack-modulus models [2–5]. In order to use the expressions developed in Part I [1] to describe the indentation crack-induced changes in Young's modulus, we shall first review the morphology of indentation cracks and then we shall modify the microcrack-modulus models to accomodate the indentation crack morphology.

## 5. Indentation cracks as an example of a model crack system

Sharp indenters (such as Vickers or Knoop) may produce an "ideal" distribution of surface microcracks, in which the number, size and spatial location of the microcracks can be controlled. However, to model an array of indentation cracks, we should consider in some detail the morphology of individual indentation cracks. The modulus–microcracking relations (Equation 3, Tables I and II) are posed in terms of $\langle A^2 \rangle$, the mean of the square of the crack size, and $\langle P \rangle$, the mean crack perimeter (Equation 4).

For Vickers indentation cracks, two idealized crack morphologies are typically cited [12, 13]: (i) "half-penny" or semi-circular radial–median crack systems, and (ii) Palmqvist cracks, consisting of a system of separate semi-elliptical cracks (see Fig. 1 for schematic diagrams of each idealized crack system). Vickers indentation-induced Palmqvist cracks have been observed in ceramics, glass–ceramics and cermets

TABLE I Microcracking–modulus relations for three-dimensional crack distributions [5][a]

| Crack geometry | $f(\nu_0)$ | $G$ | $\varepsilon$ | Orientation |
|---|---|---|---|---|
| Penny | $16(1-\nu_0^2)/3$ | $\pi a^3/2$ | $N\langle a^3 \rangle$ | Aligned |
| | $16(1-\nu_0^2(10-3\nu_0)/45(2-\nu_0)$ | | | Random |
| Half penny | $16(1-\nu_0^2)/3$ | $\pi a^3/4$ | $0.5N\langle a^3 \rangle$ | Aligned |
| | $16(1-\nu_0^2)(10-3\nu_0)/45(2-\nu_0)$ | | | Random |
| Slit | $\pi^2(1-\nu_0^2)/2$ | $2c^2l^2/(c+l)$ | $4N\langle c^2l^2 \rangle/\pi(c+l)$ | Aligned |
| | $\pi^2(1+\nu_0)(5-4\nu_0)/30$ | | | Random |
| Ellipse | $16(1-\nu_0^2)/3$ | $\pi^2bd^2/4E(k)$ | $N\pi\langle bd^2 \rangle/2E(k)$ | Aligned |
| | | | | Random |
| | $16(1-\nu_0^2)(10-3\nu_0)/45(2-\nu_0)$ | | | |
| Half-ellipse | $16(1-\nu_0^2)/3$ | $\pi^2bd^2/8E(k)$ | $N\pi\langle bd^2 \rangle/4E(k)$ | Aligned |
| | $16(1-\nu_0^2)(10-3\nu_0)/45(2-\nu_0)$ | | | Random |

[a] $\nu_0$ = Undamaged Poisson's ratio, $\langle a \rangle$ = average radius of crack for penny and halfpenny cracks, $c$ = half of average crack size for slit cracks, $l$ = depth of slit cracks, $b$ = half of major axis for elliptical and half-elliptical cracks, $d$ = half of minor axis for elliptical and half-elliptical cracks, $E(k)$ = complete elliptical integral of the second kind, $k = (b^2 - d^2)^{1/2}/b$.

TABLE II Crack geometry modifications for three-dimensional microcrack models treating aligned cracks[a]

| Crack geometry | $f(\nu_0)$ | Area | Perimeter[b] |
|---|---|---|---|
| 3D slit, unmodified | $\pi^2(1-\nu_0^2)/2$ | $2cl$ | $2c + 2l$ |
| Modified 3D slit | $\pi^2(1-\nu_0^2)/2$ | $2cl - \pi h^2/2$ | $2c + 2l + \pi h$ |
| Modified 3D slit (elliptical-indent bottom) | $\pi^2(1-\nu_0^2)/2$ | $2cl - \pi h^2 k'/2$ | $2[c + l + hE(k)]$ |
| Half-ellipse (unmodified) | $16(1-\nu_0^2)/3$ | $\pi bd/2$ | $2bE(k)$ |
| Modified half-ellipse | $16(1-\nu_0^2)/3$ | $\pi(bd - h^2)/2$ | $2bE(k) + \pi h$ |
| Modified half-ellipse (elliptical-indent bottom) | $16(1-\nu_0^2)/3$ | $\pi(bd - h^2k')/2$ | $2E(k)(b + h)$ |
| Palmqvist | $16(1-\nu_0^2)/3$ | $(\pi bd/4) - hd$ | $bE(k) + d - h$ |

[a] $\nu_0$ = Undamaged Poisson's ratio, $c$ = half of average crack size for slit cracks, $l$ = depth of slit cracks, $b$ = half of major axis for elliptical and half-elliptical cracks, $d$ = half of minor axis for elliptical and half-elliptical cracks, $h$ = half of indentation impression diagonal size, $E(k)$ = complete elliptical integral of the second kind, $k = (b^2 - d^2)^{1/2}/b$, $k' = (1 - k^2)^{1/2}$.
[b] Perimeter does not include free surface.

[14–19]. Some researchers have argued that the Palmqvist-type crack morphology occurs at low indent loads (for a $c/a$ ratio less than about 3, where the crack length $c$ and indent diagonal length $a$ are defined in Fig. 1) [14–17]. At higher indentation loads the crack morphology switches to the halfpenny type [14–17].

However, Palmqvist cracks are not necessarily limited to low-load regimes, and Palmqvist crack morphologies are not always limited to an idealized system of four semi-elliptical cracks per Vickers indent. By serial polishing, Shetty *et al.* [18, 19] observed non-ideal Palmqvist cracks generated by Vickers indentation at loads from 50 to 200 N in Corning Pyroceram 9606 glass–ceramics and at loads up to 500 N in WC–Co cermets (Fig. 2). Thus, even at relatively high loads, a well-developed radial–median crack system (a halfpenny crack) was not observed for the Pyroceram and WC–Co cermets [18, 19].

In addition to Palmqvist cracks, the halfpenny or semi-circular crack is the second idealized form of Vickers indentation crack [20, 21]. As noted above, ceramics that exhibit Palmqvist crack morphologies at low loads may develop halfpenny cracks at higher loads. Thus the halfpenny crack morphology has been termed a "fully-developed radial–median crack system". The ideal halfpenny morphology also may be disrupted by microstructural features. If a polycrystalline specimen's grain size approaches the indent impression size, then Vickers indent cracks can exhibit a number of complicated systems of multiple cracks in which the cracks tend to follow grain boundaries [22].

To accurately model a system of indentation cracks, we thus must determine the particular crack morphology, which can in fact depend on the indentation load, the specimen's microstructure, the relative load range, and a number of other factors. It is only when our assumed (or measured) crack geometry is realistic that we can utilize the flexibility of the indentation-generated cracks to test surface microcracking-modulus theories.

For both Vickers and Knoop indentations, a plastically deformed zone, commonly taken to be hemispherical in shape, is formed directly below the indentation impression (Fig. 3).

## 5.1. Difficulties and limitations in utilizing indentation cracks

From an experimental standpoint, indentation cracks are quite convenient for a study of surface-limited microcrack damage. Via indentation, a controlled array of cracks can be introduced into the specimen surface(s), where the indentation crack size, crack orientation and crack location can be controlled by the experimenter.

For a microcrack field produced by indentation at a fixed load, the thickness of the microcracked surface

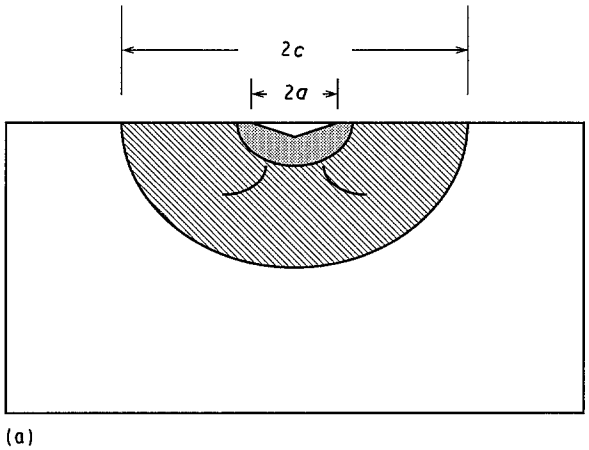


*Figure 1* Schematic diagram of idealized Vickers indentation crack morphologies: (a) the halfpenny or semi-elliptical radial–median crack system, and (b) Palmqvist cracks, consisting of a system of separate semi-elliptical cracks.

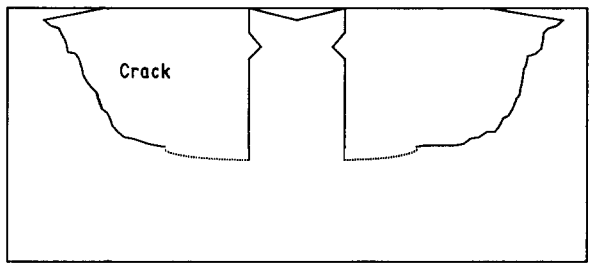


*Figure 2* An example of a non-ideal Palmqvist crack morphology (after Shetty *et al.* [19]).

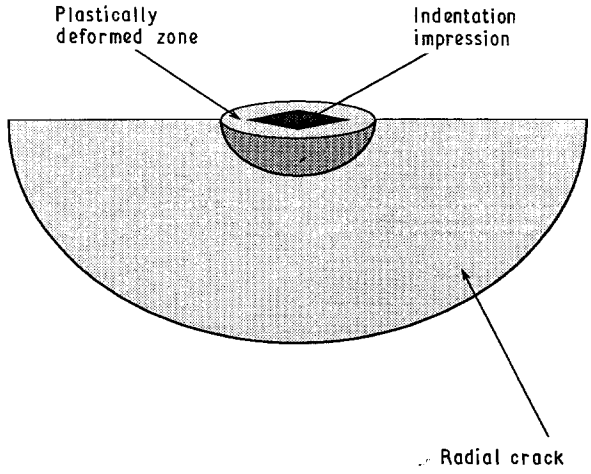


*Figure 3* Plastically deformed zone formed directly below the indentation impression.

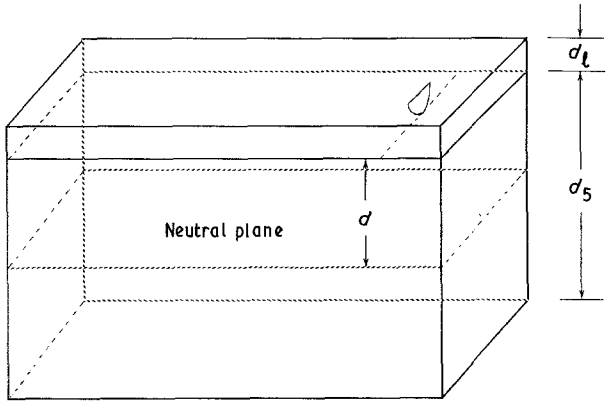


*Figure 4* For indentation cracks, a schematic diagram for a two-layer composite model showing the thickness of the microcracked surface layer, which is identical to the mean depth of the indentation cracks.

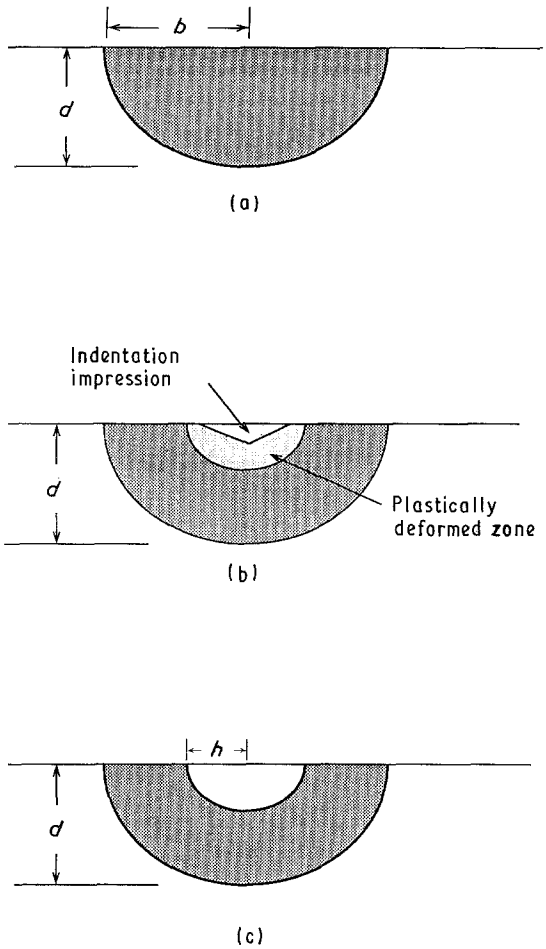


*Figure 5* (a) Idealized half-ellipse crack, (b) indentation crack, (c) half-ellipse crack modified to account for plastic zone ligament.

layer will be identical to the mean depth of the indentation cracks (Fig. 4). Thus the theories assuming a three-dimensional crack array may not be adequate to describe the modulus of the damaged layers. In addition, the indentation crack geometry does not coincide with the standard crack geometries listed in Table I. Finally, there is a residual stress field associated with indentation-induced microcracks that may alter the measured elastic modulus.

### 5.2. Modification of crack geometry expression to account for indentation crack geometry

The geometry of even fully-developed indentation cracks differs from the idealized crack geometries listed in Table I (see also the discussion in section 5). To a first approximation, indentation cracks are semi-circular or semi-elliptical rather than circular or elliptical. In addition, the faces of the indentation cracks are joined by a plastic zone ligament (Fig. 5).

For three-dimensional microcrack distributions, we choose to represent the crack geometry by the generalized geometry parameter $G = 2\langle A^2\rangle/\pi\langle P\rangle$ [2–5]. In contrast to the standard linear microcracking-modulus theories [2–5], we compute the mean of the square of the crack area $\langle A^2\rangle$ and crack perimeter $\langle P\rangle$ as they are modified by the presence of the plastically deformed zone "ligament". For an unmodified semi-elliptical crack (Table I) the mean crack area is $\pi bd/2$, where $b$ and $d$ are the semi-major and semi-minor axes of the ellipse, respectively. To account for the crack face area reduction due to the plastic zone ligament (Table II) we subtract $\pi h$, where $h$ is the radius of the ligament (plastic zone) in the plane of the semi-elliptical crack. If we assume that the plastically deformed zone has the same eccentricity as the crack, the modified crack perimeter and surface area are as shown in Table II under "modified half-ellipse, elliptical indent bottom".

Table II compares the expressions for the mean crack area and mean crack perimeter for the standard crack geometries (slit, penny and ellipse) to expressions for the same crack geometries, but as modified to account for the plastic zone ligament linking the crack faces (Fig. 5).

Alternatively, the indentation crack surface-damaged layer can be modelled as a two-dimensional crack distribution where an array of through-plate cracks are oriented normal to the plane of the plate (Appendices A and B). However, the subsurface geometry of the indentation crack (semi-circular or semi-elliptical, for example) cannot be represented by a two-dimensional model. The three-dimensional analogue of the two-dimensional slit crack distribution is a three-dimensional through-plate crack.

The two-dimensional crack models can be modified to treat the plastic zone (ligament) of the indentation crack such that an indentation crack of length $2c$ can be modelled as two separate cracks, each of length $c - a$ (Fig. 6). (The length of the indentation crack is $2c$, which includes $2a$, where $2a$ is the diagonal length of the indentation impression.)

## 6. Strategy for experimental testing

For model surface-microcrack systems, we can independently compare the predicted dependence on the crack orientation, crack geometry, layer geometry and crack number density with the experimental data.

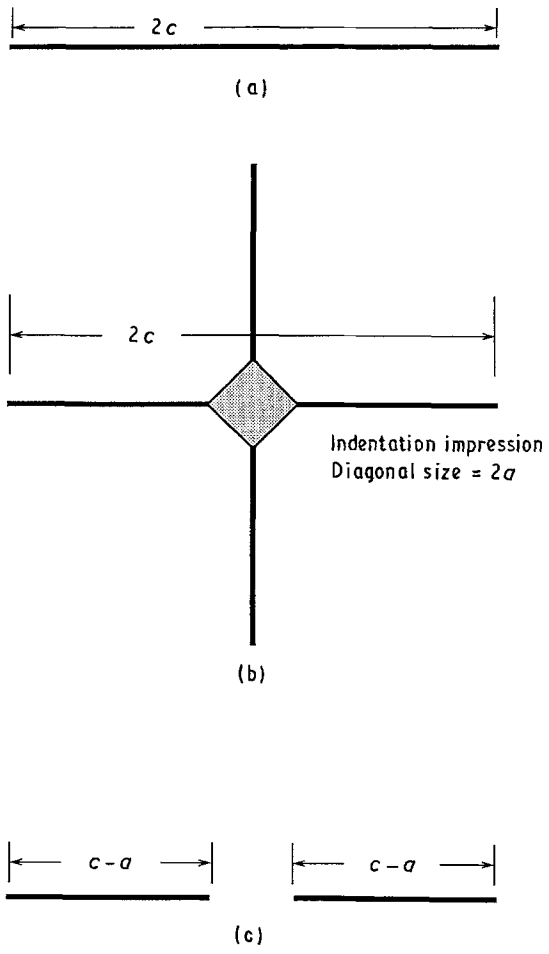


*Figure* 6 (a) Idealized two-dimensional slit crack, (b) indentation crack, (c) two-dimensional model of indentation crack.

## 6.1. *N*, the microcrack number density

For two-layer composites (one microcracked surface layer bonded to a microcrack-free layer), the fractional modulus change for both the ROM model (Equation 8 in Part I [1] and the dynamic modulus model (Equation 11 in Part I) are linear functions of the crack number density $N$, such that

$$\frac{E_s - E}{E_s} = SN \tag{5}$$

where $S$ depends on the crack alignment parameter $f$, crack geometry parameter $G$, and the microcracked layer's relative thickness. Equation 5 applies to three-layer composites if $f$ and $G$ are identical for each of two microcracked layers of equal thickness (Equation 7 in Part I for the ROM model and Equation 42 in Part I for the dynamic modulus model). Thus, for specimens containing surface microcrack populations, a plot of $(E_s - E)/E_s$ versus $N$ should be a straight line of slope $S$. In Part III [23] we test this prediction.

## 6.2. Crack and layer geometries

Surface-limited microcrack systems exhibit two geometrical hierarchies, one based on the average microcrack geometry and the second on the damaged-layer geometry [1]. In this section, we fix the layer geometry by assuming a constant value for the ratio of the thickness of the damaged layer(s) to that of the specimen. Also, we shall label two nominally identical microcracked specimens as specimens I and II. Furthermore, we assume that the initial (undamaged) Poisson's ratio is identical for specimens I and II and that the induced crack systems in specimens I and II have the same alignment*.

Specimen I is damaged by cracks of mean area $\langle A_I \rangle$ and mean crack perimeter $\langle P_I \rangle$. Specimen II is damaged by cracks of mean area $\langle A_{II} \rangle$ and mean perimeter $\langle P_{II} \rangle$. Thus the relative slopes $S_I/S_{II}$ of the $(E_s - E)/E_s$ versus $N$ plots will be given by

$$\frac{S_I}{S_{II}} = \frac{\langle A_I^2/P_I \rangle}{\langle A_{II}^2/P_{II} \rangle} \tag{6a}$$

which is a function of crack geometry only‡.

In particular, if specimens I and II contain semi-elliptical microcracks of mean semi-minor axis lengths $d_I$ and $d_{II}$ and mean semi-major axis lengths $b_I$ and $b_{II}$, the relative slope will be given by

$$\frac{\langle A_I^2/P_I \rangle}{\langle A_{II}^2/P_{II} \rangle} = \left[\frac{(\pi b_I d_I/2)^2}{2b_I E(k_I)}\right]\left[\frac{2b_{II}E(k_{II})}{(\pi b_{II}d_{II}/2)^2}\right]$$

$$= \left[\frac{b_I d_I^2}{b_{II}d_{II}^2}\right]\left[\frac{E(k_{II})}{E(k_I)}\right] \tag{6b}$$

where $E(k)$ = complete elliptical integral of second kind and

$$k_I = \frac{(b_I^2 - d_I^2)^{1/2}}{b_I}$$

$$k_{II} = \frac{(b_{II}^2 - d_{II}^2)^{1/2}}{b_{II}}$$

If the eccentricities of semi-elliptical cracks I and II are the same, then $E(k_I) = E(k_{II})$ and Equation 6b becomes

$$\frac{\langle A_I^2/P_I \rangle}{\langle A_{II}^2/P_{II} \rangle} = \frac{b_I d_I^2}{b_{II}d_{II}^2} \tag{6c}$$

If both crack I and crack II are semi-circular (that is $b_I = d_I = r_I$ = radius of crack I and $b_{II} = d_{II} = r_{II}$ = radius of crack II), then $k_I = k_{II} = 0$ and $E(k_I) = E(k_{II}) = \pi/2$ and Equation 6b becomes

$$\frac{\langle A_I^2/P_I \rangle}{\langle A_{II}^2/P_{II} \rangle} = \frac{r_I^3}{r_{II}^3} \tag{6d}$$

For slit cracks of length $2a_I$ and $2a_{II}$, and crack depths $d_I$ and $d_{II}$, the relative slope will be

$$\frac{\langle A_I^2/P_I \rangle}{\langle A_{II}^2/P_{II} \rangle} = \left[\frac{(2a_I d_I)^2}{2(a_I + d_I)}\right]\left[\frac{2(a_{II} + d_{II})}{(2a_{II}d_{II})^2}\right]$$

* From Table I, note that the crack orientation function $f$ is a function of the Poisson's ratio $\nu_0$ of the undamaged state of the specimen.

‡ Identical crack layer geometries were assumed for specimens I and II, thus the ratio of the layer geometry polynomials for I and II will become unity [1]. Comparing specimens with differing layer geometries would mean that Equation 5 would include the ratio of the appropriate layer geometry polynomials [1].

$$= \left[\frac{(a_I d_I)^2}{(a_{II} d_{II})^2}\right]\left[\frac{(a_{II} + d_{II})}{(a_I + d_I)}\right] \quad (7a)$$

If for a slit crack, the crack length is twice the crack depth (which is analogous to the semi-circular crack where the crack length – or twice the crack radius – is twice the crack depth), then $a_I = d_I = \alpha$ and $a_{II} = d_{II} = \beta$, thus Equation 7a becomes

$$\frac{\langle A_I^2/P_I\rangle}{\langle A_{II}^2/P_{II}\rangle} = \frac{\alpha^4}{\beta^4}\left(\frac{2\beta}{2\alpha}\right) = \frac{\alpha^3}{\beta^3} \quad (7b)$$

Thus using experimentally determined mean crack sizes and geometries of two specimens containing model crack systems, the relative slope $S_I/S_{II}$ can be predicted uniquely, without reference to the crack number density or the crack alignment (if the crack orientation is the same in the two cases).

As a particular example, consider cracks in specimen I to have an experimentally observed mean surface crack length $\langle \ell_I \rangle$. Cracks in specimen II have an experimentally observed mean surface crack length $\langle \ell_{II} \rangle = \langle \ell_I \rangle/2$. If the cracks in specimens I and II were semi-circular, then the relative slope of $(E_s - E)/E_s$ versus $N$ would be 8 (according to Equation 6c). If the cracks in both specimens were slit cracks in which the length of the crack's surface trace was twice the crack depth, then the relative slope of $(E_s - E)/E_s$ versus $N$ would be 8 also (according to Equation 7b).

### 6.3. Crack orientation

If microcrack damage of similar crack geometry and size, but differing crack orientation, is induced in two nominally identical specimens, then the crack orientation function $f(\nu_0)$ may be tested independently of the crack geometry and crack number density. For example, if cracks of mean area $\langle A \rangle$ and mean perimeter $\langle P \rangle$ were induced in both specimens I and II, but microcracks in specimen I were randomly oriented and microcracks in specimen II were aligned, then $S_I/S_{II}$, the ratio of the $(E_s - E)/E_s$ versus $N$ slopes is given by $f(\nu_0)_a/f(\nu_0)_r$, where the subscripts a and r refer to "aligned" and "random" crack orientation, respectively. For example, for elliptic microcracks of fixed geometry, the relative slope would be (see Table I)

$$\frac{f(\nu_0)_a}{f(\nu_0)_r} = \frac{16(1 - \nu_0^2)/3}{16(1 - \nu_0^2)(10 - 3\nu_0)/45(2 - \nu_0)} = \frac{15(2 - \nu_0)}{(10 - 3\nu_0)} \quad (8)$$

while for slit cracks of fixed geometry, the relative slope would be written as

$$\frac{f(\nu_0)_a}{f(\nu_0)_r} = \frac{\pi^2(1 - \nu_0^2)/2}{\pi^2(1 + \nu_0)(5 - 4\nu_0)/30} = \frac{15(1 - \nu_0^2)}{(1 + \nu_0)(5 - 4\nu_0)} \quad (9)$$

For $\nu_0 = 0.25$, the numerical values of $f(\nu_0)_a/f(\nu_0)_r$ are 2.838 and 2.813, respectively, for the elliptical and the slit cracks. Thus, the relative slope of the $(E_s - E)/E_s$ versus $N$ plots could be predicted prior to performing the experiment, thus providing a check on the alignment factors independent of crack geometry and crack number density.

## 7. Summary

In Part I [1] we developed expressions for the fractional change in modulus due to surface-limited microcracks. Part I gives the modulus change in terms of the geometry of the microcracked layer and in terms of general factors $f$ (crack alignment), $G$ (crack geometry) and $N$ (crack number density), where $f$ and $G$ can be expressed in terms of a number of existing modulus-microcracking theories [2–5] . This paper considers the application of the models developed in Part I to particular crack geometries.

For the case of model indentation crack distributions, modifications were made to the crack perimeter and area calculations to account for the ligament bridging the two crack faces in an indentation crack.

Experimentally [23], the fractional modulus change of specimens subjected to indentation-crack damage is described well by three-dimensional crack models modified to account for the plastic zone ligament.

In addition, this paper discusses approaches for experimentally testing the predictions of the ROM and dynamic modulus models. Part III [23] represents experimental data on a model indentation crack system in polycrystalline alumina and compares the experimental data with expressions developed in Part I and in this paper.

## Appendix A: A relation between expressions for two-dimensional through-plate slit cracks in plates and three-dimensional slot cracks in surface-damaged bars

For aligned slit cracks in three dimensions, the Young's modulus normal to slits, $E$, is (Table I, [5] )

$$\frac{E}{E_0} = 1 - fGN = 1 - 2\pi(1 - \nu_0^2)\frac{a^2 l^2 N}{a + l} \quad (A1)$$

For cracks of length $2a$ and depth $l$, $G$ becomes $2[4a^2l^2/2(a + l)]/\pi$ and $f = \pi^2(1 - \nu_0^2)/2$. This expression for $G$ assumes that the crack perimeter $\langle P \rangle$ does not include the single free surface of the slit crack (Equation 4).

For a plate of surface area $A$ and thickness $t$, the volumetric crack number density $N$ equals $n/At$ where $n$ is the number of cracks in the specimen and $At$ is the specimen volume. If we express $t$ in terms of a constant multiple $k$ of the crack depth $l$, then $t = kl$ and Equation A1 becomes

$$\frac{E}{E_0} = 1 - 2\pi(1 - \nu_0^2)\frac{a^2 l}{a + l}\left(\frac{n}{Ak}\right) \quad (A2)$$

As the crack depth $l$ approaches the plate thickness (that is, $k \to 1$), the crack becomes a through-slot type

crack with length $2a$ and depth $l$:

$$\lim_{k\to 1}\frac{E}{E_0} = 1 - 2\pi(1-\nu_0^2)\frac{a^2 l}{a+l}\left(\frac{n}{A}\right) \quad \text{(A3)}$$

If we ignore both of the free surfaces of the slot crack through the plate, then Equation A3 becomes

$$\lim_{k\to 1}\frac{E}{E_0} = 1 - 2\pi(1-\nu_0^2)\frac{a^2 l}{l}\left(\frac{n}{A}\right)$$
$$= 1 - 2\pi(1-\nu_0^2)a^2 N_a \quad \text{(A4)}$$

where $N_a = n/A$ is the crack number density per unit surface area. If the crack field is sufficiently dilute that the factor $2\pi(1-\nu_0^2)a^2 N_a$ is small compared to unity, then using the geometric series expansion of Equation A4 and retaining only the terms of order $O(N_a)$ gives

$$\frac{E}{E_0} \approx \frac{1}{1+2\pi(1-\nu_0^2)a^2 N_a} \quad \text{(A5)}$$

which is identical to the expression obtained by Hasselman and Singh [24] for dilute two-dimensional aligned crack distributions (Appendix B, Equation B3).

## Appendix B: Two-dimensional models of aligned, through-plate cracks – aligned two-dimensional crack models

Two-dimensional microcrack-modulus models typically treat an array of through-plate cracks oriented normal to the plane of the plate [24–26]. Based on Yokobori and Ichikawa's expression for the strain energy of coplanar rows of through-plate cracks under plane strain conditions [25], Hasselman and Singh [24] expressed the effective Young's modulus of the plate normal to the plane as (Fig. B1).

$$E = \frac{E_0}{[1-\{16N_a h^2(1-\nu_0^2)\ln[\cos(\pi a/2h)]\}/\pi]} \quad \text{(B1)}$$

where $E_0$, $\nu_0$ = undamaged Young's modulus and Poisson's ratio, respectively, $N_a$ = number density of cracks per unit area, $a$ = half-length of the crack and $h$ = half of transverse intercrack spacing. For a very dilute crack number density (when $N \to 0$, $h \to \infty$), $\ln[\cos(\pi a/2h)]$ may be approximated as [27]

$$\ln\left[\cos\left(\frac{\pi a}{2h}\right)\right] = -\frac{(\pi a/2h)^2}{2} - \frac{(\pi a/2h)^4}{12} - \frac{(\pi a/2h)^6}{45} - \frac{17(\pi a/2h)^8}{2520} \quad \text{(B2)}$$

In the dilute crack number density approximation where $h > a$, only the first term of Equation B2 is retained, so that Equation B1 becomes

$$E = \frac{E_0}{1+2\pi N_a(1-\nu_0^2)a^2} \quad \text{(B3)}$$

where all parameters are as defined in Equation B1.

Delameter *et al.* [26] derived the effective Young's modulus, $E$, for a sheet under plane stress conditions

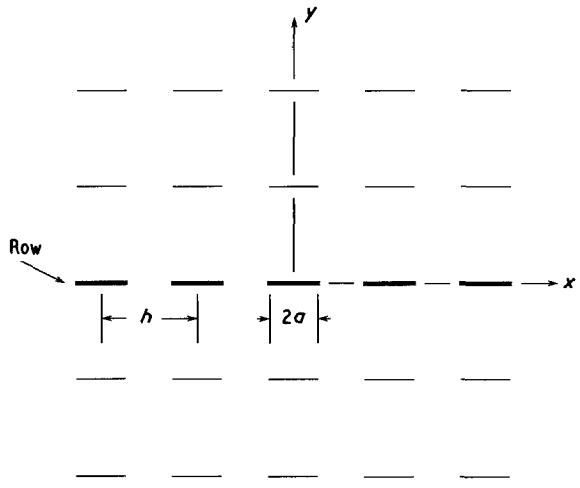


*Figure B1* Schematic diagram of a plate with a rectangular array of cracks with a transverse intercrack spacing of $2h$, as modelled by Hasselman and Singh [24].

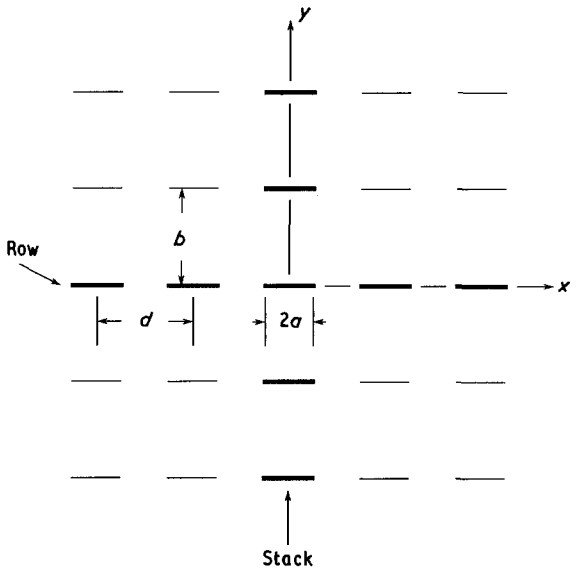


*Figure B2* Flat plate with a doubly periodic rectangular array of cracks, having rows and stacks (after Delameter *et al.* [26]).

containing a rectangular array of through-plate cracks oriented normal to the plane of plate (Fig. B2) as

$$E = \frac{E_0}{1+(2\pi a^2 B_1^1/bd)} \quad \text{(B4)}$$

where $E_0$ = undamaged Young's modulus, $a$ = half-length of the crack, $d$ = transverse intercrack spacing and $B_1^1 = 2(d/\pi a)^2 \ln[\sec(\pi a/d)]$. When $d \gg a$, $B_1^1$ approaches unity. Also $1/bd$ is equivalent to $N_a$, the number density of cracks per unit area. Thus for the dilute crack case, Equation B4 becomes

$$E = \frac{E_0}{1+2\pi a^2 N_a} \quad \text{(B5)}$$

For a dilute array of through-plate cracks, the expressions of Hasselman and Singh [24] and Delameter *et al.* [26] differ only by a factor of $(1-\nu_0^2)$.

## References


1. E. D. CASE and Y. KIM, *J. Mater. Sci* **28** (1993) 1885.
2. B. BUDIANSKY and R. J. O'CONNELL, *Int. J. Solids Struct.* **12** (1976) 81.
3. R. L. SALGANIK, *Mech. Solids* **8** (1974) 135.
4. A. HOENIG, *Int. J. Solids Struct.* **15** (1979) 137.
5. N. LAWS and J. R. BROCKENBROUGH, *ibid.* **23** (1987) 1247.
6. J. R. WILLIS, *Adv. Appl. Mech.* **21** (1981) 1.
7. E. D. CASE, *J. Mater. Sci.* **11** (1984) 3702.
8. E. D. CASE and C. J. GLINKA, *ibid.* **19** (1984) 2962.
9. J. J. MECHOLSKY Jr, S. W. FREIMAN and R.W. RICE, *J. Amer. Ceram. Soc.* **60** (1977) 114.
10. H. P. KIRCHNER, *ibid.* **67** (1984) 127.
11. *Idem, ibid.* **67** (1984) 347.
12. C.B. PONTON and R. D. RAWLINGS, *Mater. Sci. Tech.* **5** (1989) 865.
13. *Idem, ibid.* **5** (1989) 961.
14. K. NIIHARA, R. MORENA and D. P. H. HASSELMAN, *J. Mater. Sci. Lett.* **1** (1982) 13.
15. K. NIIHARA, *ibid.* **2** (1983) 221.
16. J. LANKFORD, *J. Mater. Sci.* **16** (1981) 1177.
17. *Idem, J. Mater. Sci. Lett.* **1** (1982) 493.
18. D. K. SHETTY, A. R. ROSENFIELD and W. H. DUCKWORTH, *J. Amer. Ceram. Soc.* **68** (1985) C-282.
19. D. K. SHETTY, I. G. WRIGHT, P. N. MINCER and A. H. CLAUER, *J. Mater. Sci.* **20** (1985) 1873.
20. B. R. LAWN and E. R. FULLER, *ibid.* **10** (1975) 2016.
21. D. B. MARSHALL, *J. Amer. Ceram. Soc.* **66** (1983) 127.
22. S. S. SMITH and B. J. PLETKA, in "*Fracture Mechanics of Ceramics*", Vol 6., edited by R. C. Bradt, A. G. Evans, F. F. Lange and D. P. H. Hasselman (Plenum, New York, 1983) pp. 189–209.
23. Y. KIM, E. D. CASE and S. GAYNOR *J. Mater. Sci.* **27** (1992) 000.
24. D. P. H. HASSELMAN and J. P. SINGH, *Amer. Ceram. Soc. Bull.* **58** (1979) 856.
25. T. YOKOBORI and M. ICHIKAWA, *J. Phys. Soc. Jpn* **19** (1964) 2341.
26. W. R. DELAMETER, G. HERMANN and D. M. BARNETT, Solid by a Rectangular Array of Cracks", *J. Appl. Mech. Trans. ASME*, **43** (1975) 74.
27. I. S. GRADSHTEYN and I. M. RYZHIK, "Table of Integrals, Series and Products", (Academic, New York, 1980) p. 46.



*Received 27 April*
*and accepted 17 June 1992*